Alexandria Engineering Journal (2017) 56, 161–170

HOSTED BY

Alexandria University

Alexandria Engineering Journal

www.elsevier.com/locate/aej
www.sciencedirect.com

ORIGINAL ARTICLE

Fluid flow and heat transfer of nanofluids in microchannel heat sink with V-type inlet/outlet arrangement

Ayoub Abdollahi [a], H.A. Mohammed [b,*], Sh.M. Vanaki [c], A. Osia [d], M.R. Golbahar Haghighi [e]

[a] *Department of Mechanical Engineering, University of Auckland, 20 Symonds Street, Auckland 1010, New Zealand*
[b] *Department of Energy Engineering, Technical College of Engineering, Duhok Polytechnic University (DPU), 61 Zakho Road-1006 Mazi Qr, Duhok, Kurdistan Region, Iraq*
[c] *School of Chemistry, Physics and Mechanical Engineering, Science and Engineering Faculty, Queensland University of Technology, 2 George St, Brisbane, Queensland 4000, Australia*
[d] *Department of Thermofluids, Faculty of Mechanical Engineering, Universiti Teknologi Malaysia, 81310 UTM Skudai, Johor Bahru, Malaysia*
[e] *Department of Mechanical Engineering, School of Engineering, Persian Gulf University, Bushehr, Iran*

Received 4 June 2016; revised 27 September 2016; accepted 28 September 2016
Available online 24 October 2016

KEYWORDS

Microchannel;
Forced convection;
Heat transfer enhancement;
Nanofluids;
Laminar flow

Abstract The fluid flow and heat transfer characteristics of laminar nanofluid flow in microchannel heat sink (MCHS) with V-Type inlet/outlet arrangement are numerically studied. A constant heat flux boundary condition is applied on the base plate of MCHS and all the other surfaces of MCHS are insulated. Four different kinds of nanofluids are utilized as working fluids which are SiO_2, Al_2O_3, ZnO and CuO dispersed in pure water as a base fluid. Three different volume fractions of 1%, 1.5% and 2% and three distinctive nanoparticle diameters of 30 nm, 40 nm and 60 nm were employed. The results specify that the SiO_2 nanofluid has the uppermost heat transfer rate compared to other tested nanofluids. Increasing the nanoparticles volume fraction together with decreasing the nanoparticles diameter enhances the Nusselt number value. The pressure drop coefficient did not change significantly by using nanofluid with various volume fractions and varied nanoparticle diameters. Moreover, the results indicate that nanofluid can enhance the performance of MCHS with V-shaped inlet/outlet arrangement.

1. Introduction

With ever-changing of technology and new horizons being peered in many fields of science, innovative ways have been supported and in the case of the present study, heat transfer

* Corresponding author. Fax: +964 6 07 55 66 159.
E-mail addresses: Ayoubabdollahi@gmail.com (A. Abdollahi), Hussein.dash@yahoo.com (H.A. Mohammed).
Peer review under responsibility of Faculty of Engineering, Alexandria University.

http://dx.doi.org/10.1016/j.aej.2016.09.019
1110-0168

Nomenclature

A	cross-section area (mm^2)
C_p	specific heat capacity (J/kg K)
D_h	hydraulic diameter (4A/P) (μm)
d_p	diameter of nanoparticle (nm)
F	MCHS pressure drop coefficient (m^{-4})
H_{ch}	depth of the microchannel (m)
H_{hs}	depth of heat sink (m)
h	heat transfer coefficient (W/m^2 K)
k	fluid thermal conductivity, (W/m K)
k_s	solid thermal conductivity, (W/m K)
L_{ch}	length of microchannel, (m)
L_{hs}	length of MCHS, (m)
$\dot{m}$	mass flow rate, (kg/sec)
M	molecular weight, (g/mol)
N	Avogadro number
Nu	Nusselt number
$\overline{Nu}$	overall Nusselt number of MCHS
P	wetted perimeter (m)
p	pressure (Pa)
q_w	heat flux at base plate of MCHS (W/m^2)
Q	fluid flow rate (m^3/s)
q''	MCHS base plate heat flux (W/m^2)
Re	Reynolds number
T	temperature (K)
$T_{hs,ave}$	mean temperature of the MCHS solid part (K)
T_{ave}	mean fluid temperature (K)
T_b	fluid bulk temperature (K)
T_s	MCHS solid temperature (K)
T_{in}	fluid inlet temperature (K)
$\overline{T_w}$	local mean microchannel wall temperature (K)
u	fluid velocity in the x direction (m/s)
u_{av}	average fluid velocity in MCHS, (m/s)
v	fluid velocity in the y direction (m/s)
V	velocity (m/s)
W_{ch}	width of microchannel (m)
W_{fin}	width of microchannel wall (m)
W_{hs}	width of the MCHS (m)
w	fluid velocity in the z direction (m/s)
x, y, z	coordinate directions

Greek symbols

κ	Boltzmann constant
ρ	density (kg/m^3)
ϕ	volume fraction of nanoparticle (%)
μ	dynamic viscosity (Ns/m^2)

Subscript

eff	effective
f	fluid
nf	nanofluid
np	nanoparticle

techniques have been developed. One of the cases in which the amount of heat transfer and fluid flow has been studied prevalently, is in electronic cooling systems. With the over-increasing furtherance of computing and electronic technology and making devices smaller but faster and more reliable in quality, the heat dissipation from these products is of importance in order to keep them in their desired designation. In most of the cases the chipsets in electronic devices had been cooled using forced air flow convection so far; however, in complex devices with lots of transistors or in high performance electronic chipsets, removing heat from the system is a crucial matter that affects the performance of that system.

During the last two decades many efforts have been done to receive high rate of heat transfer from the system and among all of them, microchannel heat sink has got the most consideration due to its small dimension and volume for each heat load but its ability of providing high heat transfer coefficient. Tuckerman and Pease [1] were the first researchers who worked on heat sink by introducing an approach for removing heat from a chip by forcing coolant over closed channels etched onto the backside of a silicon wafer. They stated that the heat transfer coefficient has a reverse proportionality with the channel width. The studies performed in this area are divided into three categories: theoretical, numerical and experimental studies. Knight et al. [2] performed a study to find an optimum heat transfer from the hot surface to the incoming fluid for both laminar and turbulent flow theoretically. They stated that for low pressure loss in the channel, the laminar flow has less thermal resistance than the turbulent one. At the opposite side, the thermal resistance is low in the turbulent region when the pressure drop is considerable.

Zhao and Lu [3] presented analytical approaches for heat transfer in a microchannel heat sink called porous medium and fin model. They concluded from their approaches that the Nusselt number increased with the channel aspect ratio increment and decreased with the increase of the effective thermal conductivity ratio. Another analytical study was on modelling of heat transfer and fluid flow in a microchannel heat sink using modified Darcy model [4]. A porous wall condition was selected as the heat sink material for the microchannel. Numerical studies were also conducted such as what Fedorov and Viskanta [5] did in which fluid flow and heat transfer were studied in a three dimensional heat sink microchannel. The Navier-Stokes equations for incompressible laminar flow were applied and the numerical data were validated with experimental data by Pak and Nakayama [6], Kim et al. [7] and Kawano et al. [8,9].

Some researchers performed experimental analysis of fluid flow and heat transfer characteristics along with the numerical approaches in microchannels. Qu and Mudawar [10] studied pressure loss and heat transfer in a copper heat sink both numerically and experimentally. The data achieved from the experiment were in a good agreement with the numerical data. Another example on study in experimental field is that of Tislej et al. [11]. They analysed the heat transfer of water passing a MCHS numerically and validated the obtained results by performing an experimental study. The section of the heat sink was of triangular shape. They show that the heat transfer

can be described using the conventional Navier-Stokes and energy equations for their study. Lee et al. [12] studied the heat transfer characteristics of deionized water in a microchannel with rectangular section, experimentally to determine the reliability of the numerical data about the thermal performance of a flow in a MCHS. They show that the maximum deviation of the numerical data with the experimental ones is around 5% that was a good accommodation of the two approaches.

Other experimental studies such as Hetsroni et al. [13] were about focusing on removing heat from electronic chips used in computers by fabricating triangular microchannels with heater on one side and analysing the heat transfer and the flow field characteristics. The medium was vapour-water two phase fluid and they concluded that in case that the flow boils in the microchannel, the heat transferred out of the system shows an enhancement. Experimental investigations like what brought above were performed considerably during the time [14–17], but the need for numerical approach still exists since there are some difficulties in measuring the distribution of wall temperatures or local fluid with conventional techniques. With this point of view, numerical approach seems to be an essential tool in giving a good insight of MCHS.

Nanofluid flow can be utilized as one of passive technique for improving heat transfer due to its higher thermal conductivity comparative to pure fluid [18,19]. Recently, Nanofluid flow and heat transfer have been studied by several authors [20–30]. Sheikholeslami et al. [19,31–33] investigated the effect of variable magnetic field on nanofluid forced convective heat transfer. They revealed that heat transfer augmentation was directly affected by Reynolds number and nanoparticle volume fraction. Mohammed et al. [34–36] numerically studied the fluid flow and heat transfer characteristics of various nanofluids with various volume fractions in different MCHS shapes. It was found that heat transfer coefficient increased by increasing the nanoparticles concentration.

Finite Volume Method (FVM) is widely being used for simulating nanofluid flow heat transfer [20,37,38]. In FVM, conservation of mass, momentum, energy is ensured at each cell and it can be used in the case of unstructured mesh. Other new methods such as Lattice Boltzmann Method (LBM) scheme and Control Volume based Finite Element Method (CVFEM) were used in order to study the effect of magnetic field on natural convection of nanofluid [27]. Both methods are operative in complex geometry. LBM has simple calculation procedure and efficient implementation for parallel computation, over other conventional CFD methods. The CVFEM, moreover, uses the advantages of both finite volume and finite element methods.

According to the literature, traditional electronic cooling systems are not efficient enough to meet the needs of the developed high circuitry systems. Besides, it is vital to prevent hot spots in the processors in order to have a reliable computer chip since hot spots in the processors decrease the efficiency of computer chips. Therefore, a great trend of research has been dedicated to improve the microchannel heat sinks (MCHSs) as an effective device for heat removal from microelectronic systems. Moreover, recent research on microchannels involved conventional fluid and there is no work stated in the available literature employing nanofluids in microchannel heat sink with V-typed inlet/outlet arrangement. It should be noted that the effects of using nanofluids flow on heat transfer characteristics and performance of microchannel heat sink with V-typed inlet/outlet arrangement have not been studied in detail previously and this has motivated the present study. The current study examines 3D laminar forced convective flow in MCHS with V-typed inlet/outlet arrangement using different nanofluids in water base fluid, different volume fractions and different nanoparticle diameters. The single-phase method is adopted. Nusselt number, an average of velocity and fluid temperature in each channel and pressure loss coefficient for laminar forced convective in MCHS with V-typed inlet/outlet arrangement are reported in order to show the effect of nanofluid on the mentioned parameters.

2. Numerical model

2.1. Physical model

The schematic diagram of MCHS with V-type inlet/outlet arrangement is shown in Fig. 1. The material of the MCHS is of silicon with the width (W_{hs}), length (L_{hs}) and height (H_{hs}) of 6.2 mm, 18 mm and 0.5 mm, respectively. The assumption is that a heat flux is generated at the bottom plate of the heat sink to simulate a condition of a CPU chip that conducts heat to the heat exchanger next to it. As shown in Fig. 1c, there are 11 channels (marked with a number from left side to right side) designed inside the heat sink when looking from the cross sectional view. The channels are created using 10 fins with wall dimensions of W_{ch} = 200 μm, L_{ch} = 10 mm, and H_{ch} = 400 μm as width, length and height, respectively. 1 mm is left at each of two ends of the first and the last channels at the cross section to provide an area to place a cover plate on the MCHS. It should be noted that the channels and the walls have the same thickness (W_{ch} = W_{fin}). There are an inlet for the flow to enter the heat sink and an outlet to let the flow out. The openings are designed with dimensions of 0.4 mm (width) and 1.8 mm (length). The distances of the inlet and outlet ports from the right wall are 0.6 mm and 1.8 mm, respectively. The flow enters from the inlet and is collected at the outlet vertically. The flow entering the test section is thermally and hydrodynamically fully developed. In constant pressure drop or Reynolds number, how to get higher heat transfer rates is important for MCHS [39,40]. The inlet boundary condition of the microchannel is set to be velocity inlet based on fixed Reynolds number (1333) with temperature of 293 K, the outlet boundary condition of the microchannel is assigned to be pressure outlet, and all the outer walls of MCHS are supposed to be insulated. The base plate is heated by a constant heat flux of 100 W/cm^2 simulating the heat generation from an electronic chip is specified.

2.2. Governing equations

In order to analyse the effect of nanofluid on fluid flow and heat transfer through MCHS with V-typed inlet/outlet arrangement, the following assumptions are considered:

i. The fluid flow and heat transfer are assumed to be steady-state.
ii. The fluid flow is laminar and single phase.
iii. The properties of fluid flow and MCHS material are constant and temperature independent.

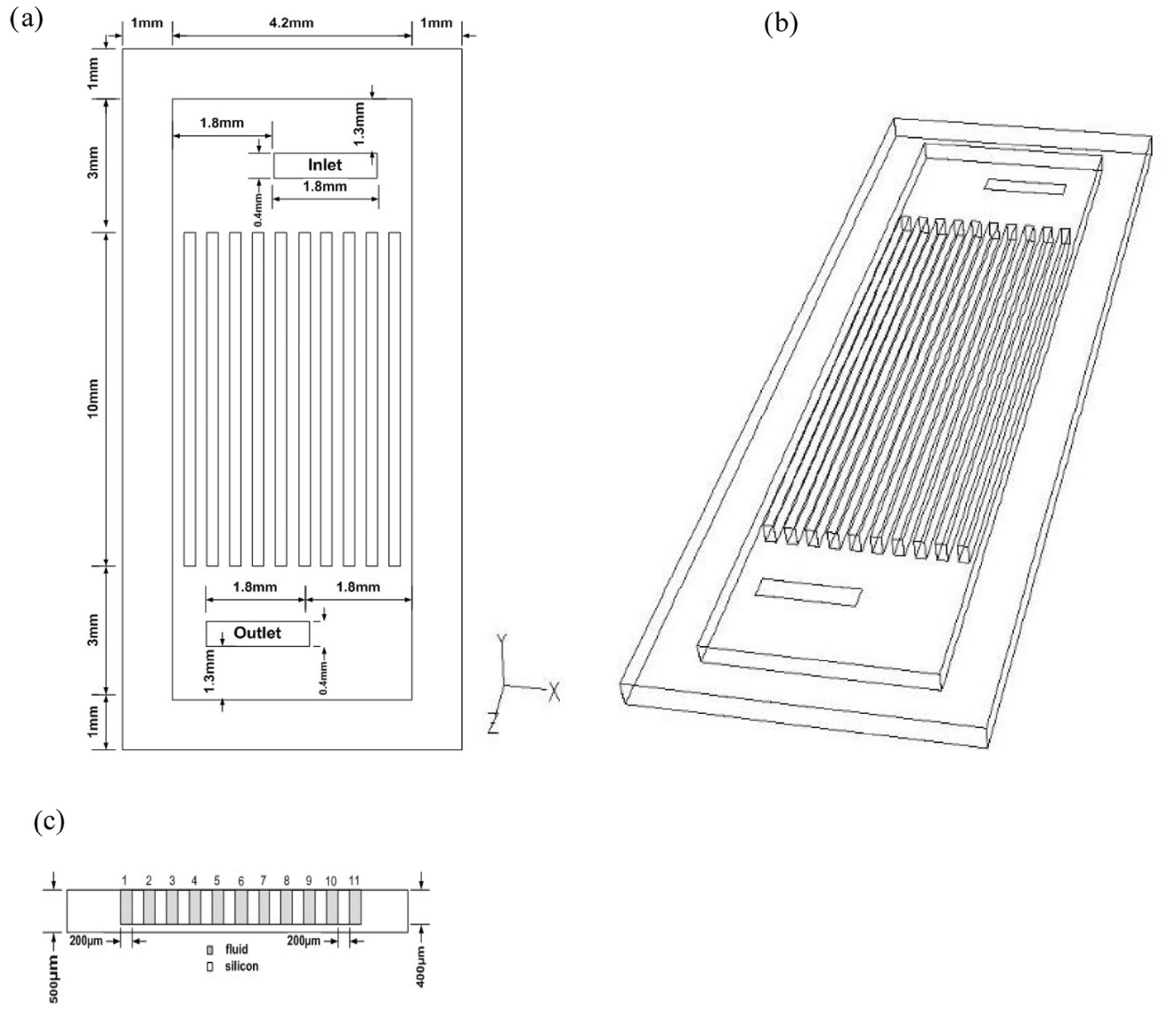

Figure 1 (a) Top view of the MCHS (Z-X plan), (b) Schematic diagram of V-typed inlet/outlet arrangement, (c) dimensions of the MCHS (X-Y plan).

The considered flow is governed via steady three-dimensional form of continuity, momentum and energy equations which can be written as follows:

Continuity equation:

$$\nabla \cdot \vec{V} = 0 \tag{1}$$

Momentum equation:

$$\rho\left(\vec{V}\cdot\nabla\cdot\vec{V}\right) = -\nabla p + \mu\nabla^2\vec{V} \tag{2}$$

Energy equation for fluid flow and solid section, respectively:

$$\rho C_P(\vec{V}\cdot\nabla T) = k\nabla^2 T \tag{3}$$

$$k_s\nabla^2 T_s = 0 \tag{4}$$

Reynolds number, local and average Nusselt number through the channel and pressure drop coefficient are calculated as follows:

$$Re = \frac{\rho u_{av} D_h}{\mu} \tag{5}$$

$$Nu = \frac{h(x)D_h}{k} = \frac{q_w D_h}{k(\overline{T_w} - T_b)} \tag{6}$$

$$\overline{Nu} = \frac{\bar{h}D_h}{k} = \frac{q_w D_h}{k(T_{hs,ave} - T_{ave})} \tag{7}$$

$$\Delta P = \frac{1}{2}\rho F Q^2 \tag{8}$$

The applied boundary conditions are given as follows:

(i) Uniform temperature and velocity profile at the inlet of microchannel.
(ii) Pressure outlet boundary condition with zero gradients at microchannel outlet.
(iii) Velocity components at the microchannel walls are zero.

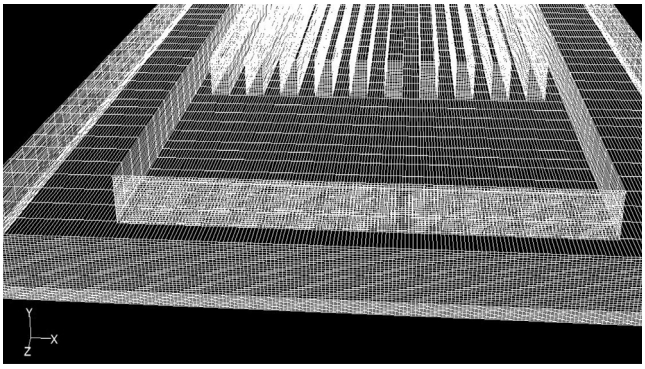

Figure 2 The grid generation used in the computation.

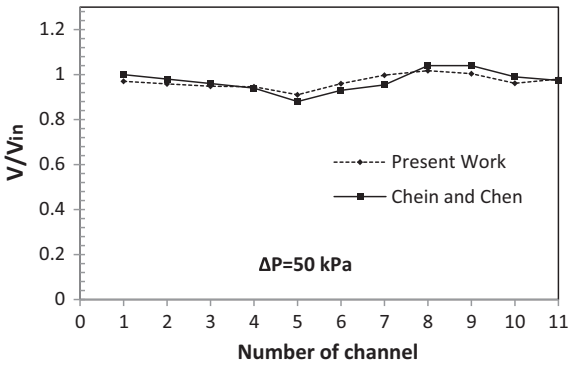

Figure 3 Averaged velocity in each channel of MCHS.

2.3. Grid independence testing

A grid independent test was done using water to find the effect of mesh size on the results. In order to choose the best grid size, three sets of hexagonal mesh were used with size of 250,000, 530,000 and 900,000. It was noticed that for three different grid sizes the value of heat sink overall heat transfer coefficient is close with error percentage of less than 2%. Hence, the mesh size of 530,000 as shown in Fig. 2 is used in order to decrease the computational time.

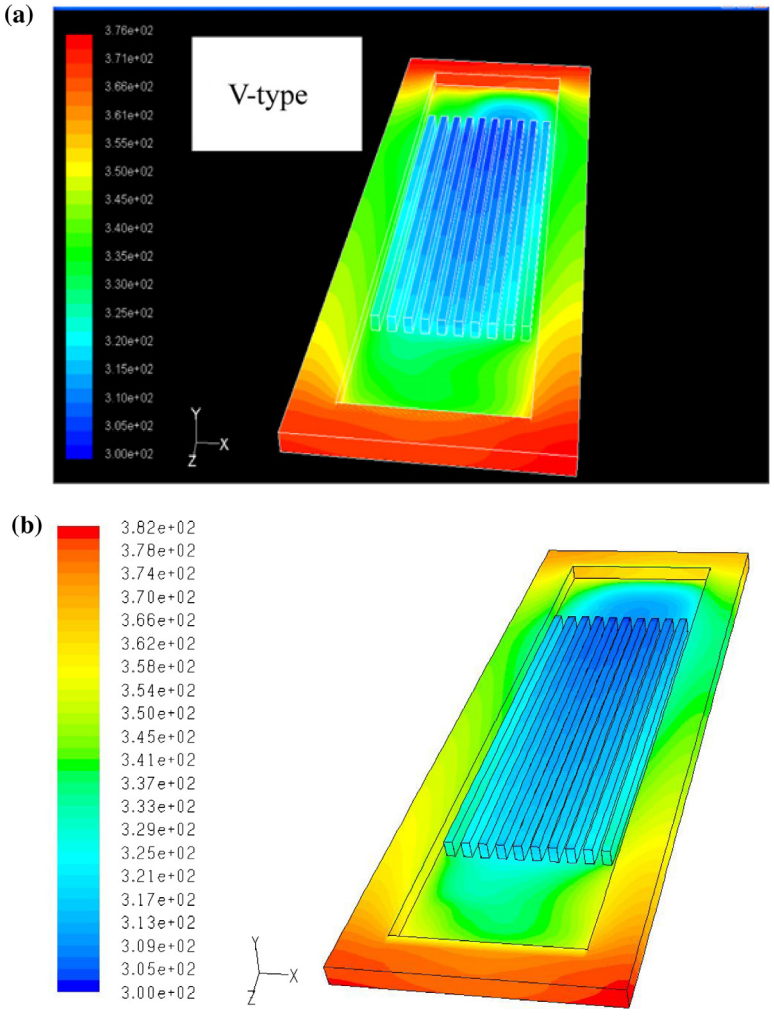

Figure 4 Temperature distribution of the solid part of MCHS. (a) Chein and Chen [41], (b) present work.

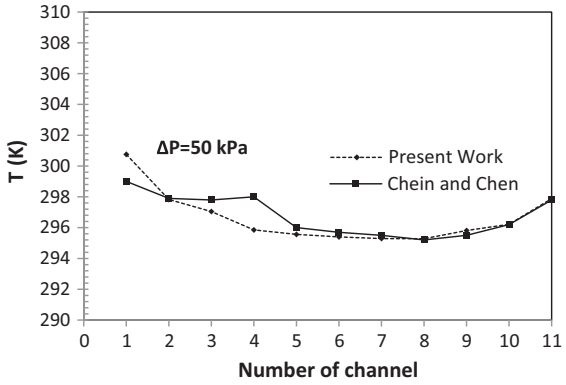

Figure 5 Comparison of the present results of averaged fluid temperature in each channel of MCHS with the results of Chein and Chen [41].

2.4. Model validation

To validate the results, a code validation of the present study was performed based on the geometry and boundary conditions of the work of Chein and Chen [41]. They analysed laminar convective heat transfer in a MCHS with V-typed inlet/outlet arrangement using water fluid flow. Figs. 3–5 show the comparison of the present results of averaged velocity in each channel, flow fields at the mid-plane of MCHS and the temperature contour of the MCHS with the results of Chein and Chen [41]. The comparison of the results of the present study with the results of Chein and Chen [41] shows a very good agreement and gives confidence to continue with the present study. Fig. 6 shows a comparison between the computed local Nusselt number along the fifth channel and Phillips [42] theoretical correlation with three-side heating correction and a good agreement between the two trends is seen.

2.5. Numerical procedures

The numerical simulation was performed by solving the governing equations (Eqs. (1)–(4)) along with the boundary conditions using finite volume method (FVM) based computational fluid dynamics (CFD) software package FLUENT 6.3.26 [43]. Both solid and fluid phases were simultaneously solved as a single domain. The SIMPLE algorithm and standard discretization are chosen to solve flow field and pressure discretization, respectively. Momentum and energy equation are approximated with the second order upwind differencing scheme. The solutions are considered to be converged when the convergence criterion values hit 10^{-6} for all variables.

2.6. Thermophysical properties of nanofluids

The thermophysical properties of nanofluid are calculated by the following equations:

Density [44]:

$$\rho_{nf} = (1-\phi)\rho_f + \phi\rho_{np} \tag{9}$$

The effective heat capacity [44]:

$$(\rho C_p)_{nf} = (1-\phi)(\rho C_p)_f + \phi(\rho C_p)_{np} \tag{10}$$

The effective thermal conductivity [45,46]:

$$k_{eff} = k_{\text{static}} + k_{\text{Brownian}} \tag{11}$$

$$k_{\text{static}} = k_f\left[\frac{(k_{np}+2k_f)-2\phi(k_f-k_{np})}{(k_{np}+2k_f)+\phi(k_f-k_{np})}\right] \tag{11.1}$$

$$k_{\text{Brownian}} = 5*10^4\beta\phi\rho_f C_{p,f}\sqrt{\frac{KT}{2\rho_{np}d_{np}}}f(T,\phi) \tag{11.2}$$

where K is Boltzmann constant ($K = 1.3807\ ^{*}\ 10^{-23}$ J/K). The values of β for different particles are given in Table 1. In order to calculate $f(T, \phi)$, the following equation is employed [47]:

$$f(T,\phi) = (2.8217*10^{-2}\phi + 3.917*10^{-3})\left(\frac{T}{T_0}\right) + (-3.0669*10^{-2}\phi - 3.91123*10^{-3})$$

The effective viscosity:

$$\mu_{eff} = \mu_f * \frac{1}{(1-34.87(dp/df)^{-0.3}*\phi^{1.03})} \tag{12}$$

$$df = 0.1\left[\frac{6M}{N\pi\rho_{fo}}\right]^{\frac{1}{3}} \tag{12.1}$$

The thermophysical properties of four varied used nanofluids with water base fluid are shown in Table 2 [48,49].

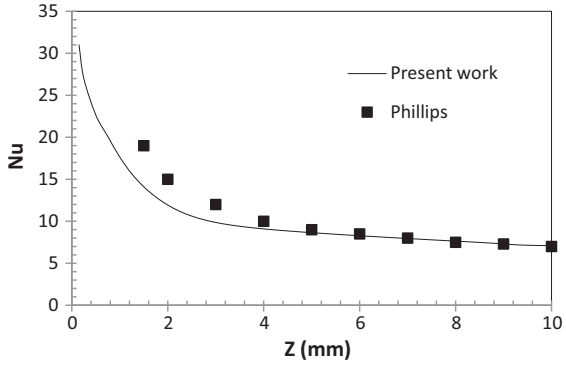

Figure 6 Comparison of computed and theoretical local Nusselt number variation along the #5 channel for V-type MCHS.

Table 1 The β values for different particles.

Type of particles	β	Concentration (%)	Temperature (K)
Al_2O_3	$8.4407(100\emptyset)^{-1.077304}$ [49]	$1 \leqslant \emptyset \leqslant 10$	$298 \leqslant T \leqslant 363$
CuO	$9.881(100\emptyset)^{-0.9446}$ [49]	$1 \leqslant \emptyset \leqslant 6$	$298 \leqslant T \leqslant 363$
SiO_2	$1.9526(100\emptyset)^{-1.4594}$ [48]	$1 \leqslant \emptyset \leqslant 10$	$298 \leqslant T \leqslant 363$
ZnO	$8.4407(100\emptyset)^{-1.077304}$ [49]	$1 \leqslant \emptyset \leqslant 7$	$298 \leqslant T \leqslant 363$

Table 2 The thermophysical properties of different nanoparticles at $T = 300$ K.

Thermophysical properties	Water	Al_2O_3	CuO	SiO_2	ZnO
$\rho\left(\frac{kg}{m^3}\right)$	998.2	3970	6500	2200	5600
$C_p\left(\frac{J}{kg\ K}\right)$	4182	765	535.6	703	495.2
$k\left(\frac{W}{m\ K}\right)$	0.6	40	20	1.2	13
$\mu\left(\frac{Ns}{m^2}\right)$	0.001003	0	0	0	0

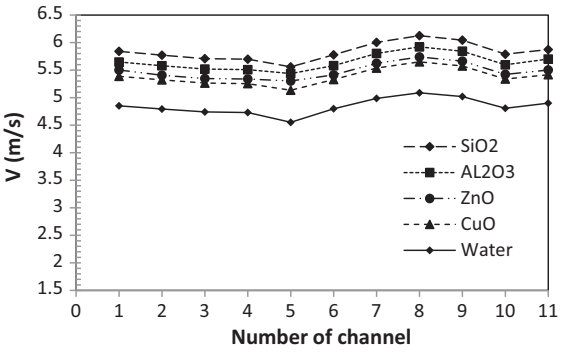

Figure 7 Averaged velocity in each channel of MCHS for different types of nanofluids.

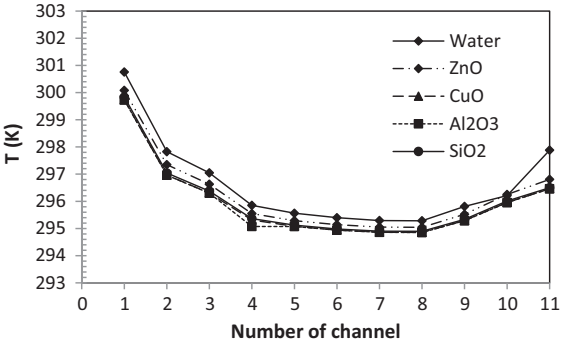

Figure 8 Averaged fluid temperature in each channel of MCHS for different types of nanofluids.

3. Results and discussion

In this section, the influence of different nanofluid types, various volume fractions and distinct nanoparticle diameters on the flow fields, thermal and performance of MCHS with V-typed inlet/outlet arrangement is investigated and discussed.

3.1. Analysis of different types of nanofluid

In this section, in order to investigate the effect of type of nanoparticles on thermal and flow fields, four types of nanofluids (SiO_2, Al_2O_3, CuO, and ZnO) with volume fraction of 2% and particle diameter of 30 nm were considered and the results were compared with pure water to show the impact of using nanofluid instead of common fluids on the heat transfer coefficient enhancement. The obtained results related to the effect of different types of nanofluids on flow and thermal fields are shown in Figs. 7 and 8, respectively.

Fig. 7 illustrates the averaged velocity in each channel of MCHS for different types of nanofluids and also pure water. As can be seen, SiO_2 nanofluid has the maximum velocity due to the lowest density among all tested nanofluids and is followed by Al_2O_3, CuO and ZnO nanofluids and finally pure water, respectively.

Table 3 lists the fluid flow rate flowing through the MCHS (Q), the pressure drop (ΔP), the pressure drop coefficient (F) and average Nusselt number of MCHS (ANN) for different nanofluids, respectively. It shows that the biggest amount of pressure loss happens when using SiO_2 nanofluid. The explanation of that is hidden in the value of the fluid density, viscosity and the fluid velocity. Viscosity has an important role on the pressure drop in the microchannel. Pure water has the lowest pressure drop due to the lowest viscosity. As shown in Table 3, the values of pressure drop coefficient for all tested nanofluids are almost close to the value of pressure drop coefficient for the pure water which is one of the most important advantages of nanofluid.

In addition, it is evident that SiO_2 nanofluid has the maximum value of ANN which is followed by CuO, Al_2O_3 and ZnO, respectively. As shown in Fig. 7, SiO_2 nanofluid has the utmost average velocity among other tested nanofluids since the density of colloidal mixture of water-SiO_2 is lower than the others. Thus, SiO_2 nanofluid has the highest ANN. In case of forced convection, the fluid velocity has a significant effect on the Nusselt number and it signifies the major reason to provide high Nusselt number.

Table 3 Results for four different nanofluids (volume fraction = 0.02 and dp = 30 nm).

Working fluid	Water	Al_2O_3	CuO	SiO_2	ZnO
Q (m^3/S)	3.60E−06	4.19E−06	4.00E−06	4.33E−06	4.06E−06
ΔP (Pa)	50597.65	72434.47	69138.37	74926.66	70153.86
F (M^{-4})	7.80828E + 12	7.8009E + 12	7.80849E + 12	7.8032E + 12	7.80463E + 12
$\overline{Nu}$	10.22144	10.39377	10.44594	10.69121	10.26665

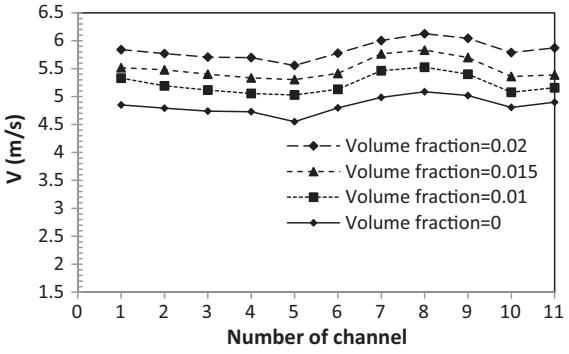

Figure 9 Averaged velocity in each channel of MCHS for SiO_2 nanofluid (dp = 30 nm) with different volume fractions.

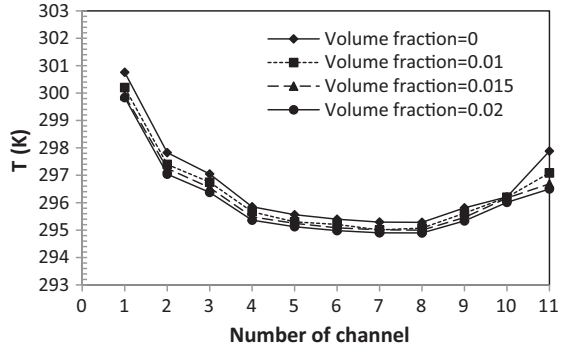

Figure 10 Averaged fluid temperature in each channel of MCHS for SiO_2 nanofluid (dp = 30 nm) with different volume fractions.

To know the fluid temperature variations related to the consequence of different working fluids, the average fluid temperature in every single channel is provided in Fig. 8. It is clear that higher average fluid temperature for removing a specific heat flux occurs when the fluid velocity is low. Following this, SiO_2 nanofluid has the highest fluid velocity and the lowest fluid temperature. In addition, the higher fluid temperature occurs in channel near the edges of MCHS because of heat transfer from high temperature edge.

3.2. Analysis of SiO_2 nanofluids volume fractions

To study the influence of different volume fractions of nanoparticles on thermal and flow fields, the range of nanoparticle concentrations of nanofluids is varied from 0% to 2%. The 0% concentration is related to pure water with no

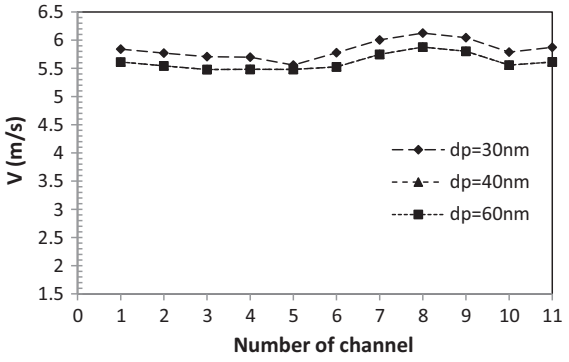

Figure 11 Averaged velocity in each channel of MCHS for SiO_2 nanofluid (volume fraction = 0.02) with different nanoparticles diameters.

nanoparticle. SiO_2 nanofluids were chosen as a working fluid since it had the best performance among all other tested working fluids. Figs. 9 and 10 show the averaged velocity and averaged fluid temperature in each channel for SiO_2 nanofluid with different volume fractions and at (dp = 30 nm), respectively.

Fig. 9 indicates that the SiO_2 nanofluid with 2% volume fraction has the highest value of velocity among all. Table 4 lists the fluid flow rate flowing through the MCHS (Q), the pressure drop (ΔP), the pressure drop coefficient (F) and ANN of heat sink for SiO_2 nanofluid with different nanoparticle concentrations. As given in this table, the pressure drop increases with the increase of volume fraction from 0% to 2%, and the SiO_2 nanofluid with 2% volume fraction has the highest pressure drop. This can be explained as the viscosity of nanofluid tends to increase with increasing nanoparticle volume fraction. The pressure drop, moreover, increases at higher velocity because of the increase of wall shear stress. It should be noted that the pressure drop coefficient values do not change considerably with increasing the SiO_2 nanofluid volume fractions.

Table 4 declares that by increasing nanofluid concentration from 0% to 2%, the ANN enhances. This is because of the energy exchange rate improvement in fluid from the anarchical nanoparticle movement [22].

In order to understand the fluid temperature variations related to the effect of different SiO_2 nanofluid volume fractions, the average fluid temperatures in every single channel are figured in Fig. 10. In removing a specific heat flux from the heat sink, a decrement of average fluid temperature was observed when SiO_2 nanofluid volume fraction increased. Therefore, it is obvious that SiO_2 nanofluid with volume fraction of 2% has better capability of heat dissipation.

Table 4 Results for SiO_2 nanofluids with different volume fractions (dp = 30 nm).

Volume fraction (%)	0	1	1.5	2
Q (m^3/S)	3.60E−06	3.90E−06	4.12E−06	4.33E−06
ΔP (Pa)	50497.65	59920.55	67190.86	74926.66
F (M^{-4})	7.79285E + 12	7.8031E + 12	7.8031E + 12	7.8032E + 12
$\overline{Nu}$	10.22143627	10.4450148	10.5759399	10.69121202

Table 5 Results for SiO_2 nanofluids at volume fraction = 2% and (dp = 30, 40, 60 nm).

dp(nm)	30	40	60
Q (m^3/S)	4.33E−06	4.16E−06	4.16E−06
ΔP (Pa)	74926.66	68928.68	68927.66
F (M^{-4})	7.8032E + 12	7.8032E + 12	7.8031E + 12
$\overline{Nu}$	10.69121202	10.63276742	10.62536895

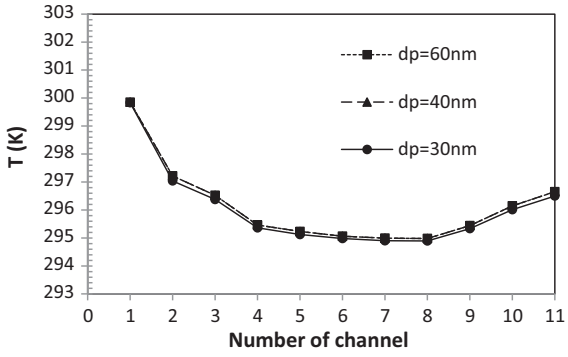

Figure 12 Averaged fluid temperature in each channel of MCHS for SiO_2 nanofluid (Volume fraction = 0.02) with different nanoparticles diameters.

3.3. Analysis of diameters of SiO_2 nanoparticles

In this section, the range of nanoparticle diameter was selected from 30 nm to 60 nm. The SiO_2 nanofluid with volume fraction of 2% was preferred as working fluid since SiO_2 (at constant volume fraction of 2%) showed better performance among all tested nanofluids.

The average velocity in each channel for SiO_2 nanofluid with different nanoparticle diameters is illustrated in Fig. 11. It is seen that the SiO_2 nanofluid with nanoparticles diameter of 30 nm has the highest value of velocity among all.

The fluid flow rate flowing through the MCHS (Q), the pressure drop (ΔP), the pressure drop coefficient (F) and ANN of MCHS for SiO_2 nanofluid with different nanoparticle diameters are given in Table 5. The nanofluid with lower nanoparticles diameter has the maximum value of pressure drop since the nanofluid viscosity has a tendency to increase with reducing nanoparticle diameter. Moreover, the pressure drop coefficient values have not changed considerably for different nanoparticle sizes.

Also, a small variation in ANN can be seen for different nanoparticle diameters. The ANN of nanofluid enhances with decreasing the nanoparticle diameter. This phenomenon is related to Brownian motion and relative surface area of nanoparticles. The smaller size of the nanoparticles has the better surface area per unit volume. The heat transfer rate is commensurate to the surface area. Therefore, the increment of effective surface area means the nanoparticles can transfer higher value of heat to the base fluid. The other reason is referred to the mean velocity of nanoparticles dispersed in the base fluid. The reduction of the size of the nanoparticles causes the higher Brownian motion velocity of the nanoparticles that increases the heat transfer rate. Therefore, the SiO_2 nanofluid with 30 nm nanoparticle size has the highest ANN and the SiO_2 nanoparticle with 60 nm diameter has the lowermost ANN.

As clarified in Fig. 12, the average fluid temperature increases when SiO_2 nanoparticles diameter increases. As a result, it is obvious that SiO_2 nanofluid with volume fraction of 2% and 30 nm nanoparticle diameter has better heat removal ability.

4. Conclusions

A numerical simulation of laminar forced convection heat transfer in MCHS with V-Type inlet/outlet arrangement was performed. The current study focused on flow field and heat transfer improvement caused by different parameters, such as different kinds of nanofluids including SiO_2, Al_2O_3, ZnO and CuO, different volume fractions of nanoparticles (0, 1, 1.5 and 2%) and different nanoparticle diameters (30, 40 and 60 nm). FVM was used to solve and discretize the governing equations. It was found that SiO_2, Al_2O_3, ZnO and CuO nanofluids in water base fluid had better heat transfer augmentation compared to pure water. The results show that SiO_2 nanofluid presents the maximum Nusselt number value among tested nanofluids and pure water. The increase of nanoparticle volume fraction enhanced the average Nusselt number. Moreover, the Nusselt number had a small enhancement with decreasing the nanoparticle diameter. Besides, the flow fluid shows that SiO_2 nanofluid had the uppermost pressure drop among tested nanofluids and pure water. Following this, the larger volume fraction and smaller nanoparticle size increase the pressure drop. No considerable effect was detected on the pressure drop coefficient in the case of using nanofluid in comparison with pure water. SiO_2 nanofluid with volume fraction of 2% and nanoparticle diameter of 30 nm had the best performance among other tested nanofluids.

References

[1] D.B. Tuckerman, R.F.W. Pease, High-performance heat sinking for VLSI, IEEE Electron Device Lett. (1981) 126–129.
[2] R.W. Knight, D.J. Hall, J.S. Goodling, R.C. Jaeger, Heat sink optimization with application to microchannels, IEEE Trans. Compon. Hybrids Manuf. Technol. 15 (1992) 832–842.
[3] C.Y. Zhao, T.J. Lu, Analysis of microchannel heat sinks for electronics cooling, Int. J. Heat Mass Transf. 45 (2002) 4857–4869.
[4] S.J. Kim, D. Kim, Forced convection in microstructures for electronic equipment cooling, J. Heat Transf. 121 (1999) 639–645.
[5] A.G. Fedorov, R. Viskanta, Three-dimensional conjugate heat transfer in the microchannel heat sink for electronic packaging, Int. J. Heat Mass Transf. 43 (2000) 399–415.
[6] D.C.B.C. Pak, W. Nakayama, Cooling of electronic systems by using manifold microchannel heat sinks, Proceedings of KSME Fall Annual Meeting, vol. 2, 1995, pp. 74–80.
[7] Y. Kim, W. Chun, J. Kim, B. Pak, B. Baek, Forced air cooling by using manifold microchannel heat sinks, KSME Int. J. 12 (1998) 709–718.
[8] K. Kawano, M. Sekimura, K. Minakami, H. Iwasaki, M. Ishizuka, Development of micro channel heat exchanging, JSME Int J., Ser. B 44 (2001) 592–598.

[9] K. Kawano, K. Minakami, H. Iwasaki, M. Ishizuka, Development of micro channels heat exchanging, in: National heat transfer symposium of Japan, 1998, pp. 45–46.
[10] W. Qu, I. Mudawar, Experimental and numerical study of pressure drop and heat transfer in a single-phase micro-channel heat sink, Int. J. Heat Mass Transf. 45 (2002) 2549–2565.
[11] I. Tiselj, G. Hetsroni, B. Mavko, A. Mosyak, E. Pogrebnyak, Z. Segal, Effect of axial conduction on the heat transfer in micro-channels, Int. J. Heat Mass Transf. 47 (2004) 2551–2565.
[12] P.-S. Lee, S.V. Garimella, D. Liu, Investigation of heat transfer in rectangular microchannels, Int. J. Heat Mass Transf. 48 (2005) 1688–1704.
[13] G. Hetsroni, A. Mosyak, Z. Segal, Nonuniform temperature distribution in electronic devices cooled by flow in parallel microchannels, IEEE Trans. Compon. Pack. Technol. 24 (2001) 16–23.
[14] T. Kishimoto, T. Ohsaki, VLSI packaging technique using liquid-cooled channels, IEEE Trans. Compon. Hybrids Manuf. Technol. 9 (1986) 328–335.
[15] M.M. Rahman, Measurements of heat transfer in microchannel heat sinks, Int. Commun. Heat Mass Transf. 27 (2000) 495–506.
[16] M. Rahman, F. Gui, Design, fabrication, and testing of microchannel heat sinks for aircraft avionics cooling, in: Intersociety Energy Conversion Engineering Conference, American Nuclear Society, 1993, pp. 1.1-1.1.
[17] T. Ravigururajan, J. Cuta, C. McDonald, M. Drost, Single phase flow thermal performance of a parallel micro-channel heat exchanger, in: American Society of Mechanical Engineers 1996 National Heat Transfer Conference, 1996.
[18] M. Sheikholeslami, M.T. Mustafa, D.D. Ganji, Effect of Lorentz forces on forced-convection nanofluid flow over a stretched surface, Particuology 26 (2016) 108–113.
[19] M. Sheikholeslami, M.M. Rashidi, D.D. Ganji, Numerical investigation of magnetic nanofluid forced convective heat transfer in existence of variable magnetic field using two phase model, J. Mol. Liq. 212 (2015) 117–126.
[20] A. Vatani, H.A. Mohammed, Turbulent nanofluid flow over periodic rib-grooved channels, Eng. Appl. Comput. Fluid Mech. 7 (2013) 369–381.
[21] M. Sheikholeslami, D.D. Ganji, M.M. Rashidi, Magnetic field effect on unsteady nanofluid flow and heat transfer using Buongiorno model, J. Magn. Magn. Mater. 416 (2016) 164–173.
[22] M. Sheikholeslami, M.M. Rashidi, T. Hayat, D.D. Ganji, Free convection of magnetic nanofluid considering MFD viscosity effect, J. Mol. Liq. 218 (2016) 393–399.
[23] M. Sheikholeslami, S. Soleimani, D.D. Ganji, Effect of electric field on hydrothermal behavior of nanofluid in a complex geometry, J. Mol. Liq. 213 (2016) 153–161.
[24] M. Sheikholeslami, D.D. Ganji, Nanofluid flow and heat transfer between parallel plates considering Brownian motion using DTM, Comput. Methods Appl. Mech. Eng. 283 (2015) 651–663.
[25] M. Sheikholeslami, D.D. Ganji, M.M. Rashidi, Ferrofluid flow and heat transfer in a semi annulus enclosure in the presence of magnetic source considering thermal radiation, J. Taiwan Inst. Chem. Eng. 47 (2015) 6–17.
[26] M. Sheikholeslami Kandelousi, KKL correlation for simulation of nanofluid flow and heat transfer in a permeable channel, Phys. Lett. A 378 (2014) 3331–3339.
[27] M. Sheikholeslami, D.D. Ganji, Entropy generation of nanofluid in presence of magnetic field using Lattice Boltzmann method, Physica A 417 (2015) 273–286.
[28] M. Sheikholeslami, D.D. Ganji, Ferrohydrodynamic and magnetohydrodynamic effects on ferrofluid flow and convective heat transfer, Energy 75 (2014) 400–410.
[29] M. Sheikholeslami, D. Ganji, Heated permeable stretching surface in a porous medium using Nanofluids, J. Appl. Fluid Mech. 7 (2014) 535–542.
[30] A. Vatani, P.L. Woodfield, D.V. Dao, A survey of practical equations for prediction of effective thermal conductivity of spherical-particle nanofluids, J. Mol. Liq. 211 (2015) 712–733.
[31] M. Sheikholeslami, K. Vajravelu, M.M. Rashidi, Forced convection heat transfer in a semi annulus under the influence of a variable magnetic field, Int. J. Heat Mass Transf. 92 (2016) 339–348.
[32] M. Sheikholeslami, M.M. Rashidi, D.D. Ganji, Effect of non-uniform magnetic field on forced convection heat transfer of Fe_3O_4–water nanofluid, Comput. Methods Appl. Mech. Eng. 294 (2015) 299–312.
[33] H. Safarnia, M. Sheikholeslami, D.D. Ganji, Electrohydrodynamic nanofluid flow and forced convective heat transfer in a channel, Eur. Phys. J. Plus 131 (2016) 1–14.
[34] H.A. Mohammed, P. Gunnasegaran, N. Shuaib, Influence of various base nanofluids and substrate materials on heat transfer in trapezoidal microchannel heat sinks, Int. Commun. Heat Mass Transf. 38 (2011) 194–201.
[35] H.A. Mohammed, P. Gunnasegaran, N. Shuaib, Numerical simulation of heat transfer enhancement in wavy microchannel heat sink, Int. Commun. Heat Mass Transf. 38 (2011) 63–68.
[36] H.A. Mohammed, P. Gunnasegaran, N. Shuaib, The impact of various nanofluid types on triangular microchannels heat sink cooling performance, Int. Commun. Heat Mass Transf. 38 (2011) 767–773.
[37] M.S. Kandelousi, Effect of spatially variable magnetic field on ferrofluid flow and heat transfer considering constant heat flux boundary condition, Eur. Phys. J. Plus 129 (2014) 1–12.
[38] H.A. Mohammed, O.A. Alawi, M.A. Wahid, Mixed convective nanofluid flow in a channel having backward-facing step with a baffle, Powder Technol. 275 (2015) 329–343.
[39] V. Leela Vinodhan, K.S. Rajan, Computational analysis of new microchannel heat sink configurations, Energy Convers. Manage. 86 (2014) 595–604.
[40] Y.-T. Yang, H.-W. Tang, W.-P. Ding, Optimization design of micro-channel heat sink using nanofluid by numerical simulation coupled with genetic algorithm, Int. Commun. Heat Mass Transf. 72 (2016) 29–38.
[41] R. Chein, J. Chen, Numerical study of the inlet/outlet arrangement effect on microchannel heat sink performance, Int. J. Therm. Sci. 48 (2009) 1627–1638.
[42] R.J. Phillips, Microchannel heat Sinks, 1987.
[43] Fluent 6 User's Guid, NH, Fluent Inc., 2000, Lebanon.
[44] J.C. Maxwell, J.J. Thompson, A Treatise on Electricity and Magnetism, Clarendon Press, Oxford, UK, 1873.
[45] A. Osia, H.A. Mohammed, A. Abdollahi, J.A. Ali, Laminar nanofluid flow over periodic two dimensional rectangular baffled channels, J. Comput. Theor. Nanosci. 11 (2014) 1018–1030.
[46] S.M. Vanaki, P. Ganesan, H.A. Mohammed, Numerical study of convective heat transfer of nanofluids: a review, Renew. Sustain. Energy Rev. 54 (2016) 1212–1239.
[47] S.M. Vanaki, H.A. Mohammed, A. Abdollahi, M.A. Wahid, Effect of nanoparticle shapes on the heat transfer enhancement in a wavy channel with different phase shifts, J. Mol. Liq. 196 (2014) 32–42.
[48] H.A. Mohammed, A.N. Al-Shamani, J.M. Sheriff, Thermal and hydraulic characteristics of turbulent nanofluids flow in a rib-groove channel, Int. Commun. Heat Mass Transf. 39 (2012) 1584–1594.
[49] R.S. Vajjha, D.K. Das, Experimental determination of thermal conductivity of three nanofluids and development of new correlations, Int. J. Heat Mass Transf. 52 (2009) 4675–4682.